RESEARCH ARTICLE

NANO · MICRO small
www.small-journal.com

Power Scavenging Microsystem for Smart Contact Lenses

Erfan Pourshaban, Mohit U. Karkhanis, Adwait Deshpande, Aishwaryadev Banerjee, Md Rabiul Hasan, Amirali Nikeghbal, Chayanjit Ghosh, Hanseup Kim, and Carlos H. Mastrangelo**

On-the-eye microsystems such as smart contacts for vision correction, health monitoring, drug delivery, and displaying information represent a new emerging class of low-profile (≤ 1 mm) wireless microsystems that conform to the curvature of the eyeball surface. The implementation of suitable low-profile power sources for eye-based microsystems on curved substrates is a major technical challenge addressed in this paper. The fabrication and characterization of a hybrid energy generation unit composed of a flexible silicon solar cell and eye-blinking activated Mg–O_2 metal–air harvester capable of sustainably supplying electrical power to smart ocular devices are reported. The encapsulated photovoltaic device provides a DC output with a power density of 42.4 μW cm^{-2} and 2.5 mW cm^{-2} under indoor and outdoor lighting conditions, respectively. The eye-blinking activated Mg–air harvester delivers pulsed power output with a maximum power density of 1.3 mW cm^{-2}. A power management circuit with an integrated 11 mF supercapacitor is used to convert the harvesters' pulsed voltages to DC, boost up the voltages, and continuously deliver ≈150 μW at a stable 3.3 V DC output. Uniquely, in contrast to wireless power transfer, the power pack continuously generates electric power and does not require any type of external accessories for operation.

1. Introduction

Autonomous health management microsystems, particularly smart contact lenses, can be employed for noninvasive communication of physiological signals such as blood glucose level[1,2] and intraocular pressure for glaucoma care.[3] These IoT devices are also used to address eye dryness,[4,5] chronic ocular surface inflammation,[6] and vision malfunctions.[7,8] Although on-the-eye ocular microdevices have a wide range of health and information applications, potentially spawning massive new markets, the lack of reliable and stand-alone power supply for these devices remains a grand challenge.

Many ocular microdevices rely on external power sources either through wired or wireless connections. For example, Chu et al.[9] developed a smart contact lens for glucose detection and successfully tested it on a rabbit's eye but the device required a wired connection to an external power source, which is not a practical approach to commercialize a wearable and mobile electronic device. Electrical power can also be delivered[2,10–16] to ocular devices wirelessly in a less obstructive manner. Wireless power transfer requires both an external transmitter antenna and an on-the-eye coil. Wireless power transfer efficiency for these systems is generally low (<10% for 10 mm distance between antennas),[2,11] but more importantly, such system needs obtrusive external components and accessories placed on or near the face of the subject.

A much more user-friendly system can be realized if energy is scavenged or generated directly on the surface of the eye instead of being transferred there. Energy generation methods utilizing photovoltaics,[17–20] biofluid electrochemistry,[21–23] and muscle movement[24,25] do not require any external connections and these techniques can be combined to supply energy in a multiplicity of modalities.

In this work, we merged two different energy generation devices, consisting of a bank of flexible silicon solar cells and an eye-blinking activated Mg–O_2 harvester to produce a power pack that supplies electric energy to a smart contact lens. The bank of flexible photovoltaics was implemented by connecting eight rigid single crystalline silicon solar cells (1.5 × 1.5 × 0.1 mm^3) in series to achieve flexibility and a high open circuit voltage (V_{oc}). The bank is next encapsulated using PDMS. The silicon solar cell bank exhibits the maximum power density of 42.4 μW cm^{-2} and 2.5 mW cm^{-2} under indoor and outdoor lighting conditions, respectively. Based on the principle of metal–air batteries,[21] we have exploited natural eye-blinking motion as a secondary source of energy generation. This eye-blinking activated Mg–O_2 energy

E. Pourshaban, M. U. Karkhanis, A. Deshpande, A. Banerjee, M. R. Hasan, A. Nikeghbal, C. Ghosh, H. Kim, C. H. Mastrangelo
Department of Electrical and Computer Engineering
University of Utah
Salt Lake City, UT 84112, USA
E-mail: erfan.pourshaban@utah.edu; carlos.mastrangelo@utah.edu

The ORCID identification number(s) for the author(s) of this article can be found under https://doi.org/10.1002/smll.202401068

DOI: 10.1002/smll.202401068

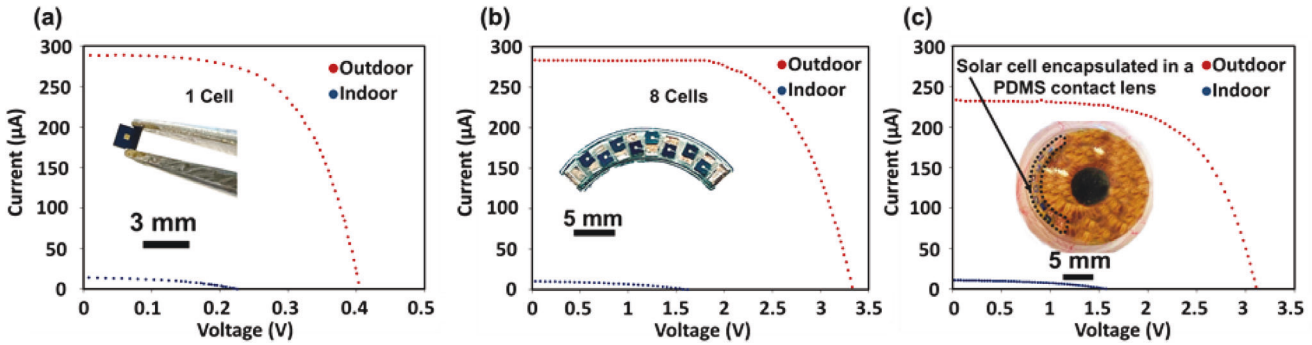

Figure 1. Optoelectronic properties of the flexible silicon solar cells under indoor and outdoor lighting conditions; a) one individual cell, b) series connections between ten cells, and c) flexible silicon solar cell encapsulated in a PDMS contact lens.

source plays a critical role in low-intensity lighting environments where the solar cell bank output is low. The electrochemical harvester delivers pulsed output with the V_{oc} and short circuit current (I_{sc}) of 2.2 V and 1.4 mA under natural eye-blinking motion.

The two energy sources were integrated with an energy storage unit and a power management circuit to provide a 3.3 V DC output with different amounts of power (from hundreds of μW to mW), that can be used both under steady power and burst modes. All microsystem components were encapsulated and conformally mounted on a curved shell testing platform that emulates the scleral region of a human eyeball. Our measurements demonstrate that this on-the-eye energy source can provide a sufficient amount of power to a liquid crystal Fresnel lens (power consumption ≈2.6 μW),[26] a distance ranging magnetometer sensor (20.79 μW at 3.3 V), and an I2C readout for continuous data transfer (13.2 μW at 3.3 V)[27] necessary to operate smart contact lenses for vision correction. Furthermore, according to D. H. Keum and the coworkers' measurements, a drug delivery system, a diabetic sensor, and a readout sensor consume 0–9, 0–30, and 34.4 μW of electric power, respectively.[2] Thus, our power pack can keep these components functional, as well.

2. Results

2.1. Flexible Silicon Solar Cell Bank

We utilized silicon solar cells because silicon cells are biocompatible,[28] exhibit a much longer lifetime,[29] and do not degrade significantly with moisture and sunlight exposure, unlike flexible organic and perovskite solar cells.[30] As shown in **Figure 1**, eight individual silicon solar cells are connected in series, mounted on a flexible substrate, and encapsulated with PDMS. Besides flexibility, the series connection cells produce a higher bank V_{oc} that is above the 1.8 V cold start-up voltage of the power management chip. Under one sunlighting condition (100 mw cm^{-2}), results show the V_{oc} and I_{sc} of 407 mV and 289 μA for an individual cell (Figure 1a). As provided in Figure 1b, the series connections between eight individual cells boost up the V_{oc} to 3.35 V delivering the maximum power of 601.2 μW. Note that the I_{sc} slightly drops, which is due to the connection's loss.

Figure 1c shows that the power conversion efficiency (PCE) reduces by 25% after PDMS encapsulation. However, the PDMS encapsulation is not only essential to prevent mechanical degradation while the device is bent but also hinders direct contact between human beings' eyelids and silicon solar cells. This device provides V_{oc} and a maximum power of 3.2 V and 448 μW under outdoor lighting conditions. These values drop to 1.6 V and 7.63 μW under indoor lighting conditions. In addition to the eye blinking capacitor charging mode, the solar cells can rapidly charge the storage capacitor using a LED recharge box. The high-intensity LED recharge box provides a rapid (450 s to charge up an 11 mF supercapacitor from 0 to 2.8 V) wireless and contactless power pack capacitor charging (Figure S1, Supporting Information).

2.2. Eye Blinking Activated Mg–O_2 Harvester

The eye-blinking activated Mg–O_2 harvester works based on the principle of metal–air batteries. As schematically illustrated in **Figure 2**, the activation mechanism of this harvester that uses eye tears as the electrolyte during natural eye blinking motion comprises three main steps. First, the harvester is in off-mode, where the electrolyte is not in contact with any part of the device, which corresponds to the completely open eyelid. Then the electrolyte goes into contact with the anode metal, leading to spontaneous oxidation reactions and the generation of electrons (eyelid half-closed). Last, the electrolyte goes into contact with both electrodes resulting in energy generation due to the oxidation reactions on the surface of the anode and oxygen reduction reactions on the cathode's surface (see Supporting Information for detailed chemical reactions). It should be emphasized that this harvester is functional because the eye tear is produced by lacrimal glands located underneath the eyelid and passes over the surface of the eyeball during every blinking cycle.[31,32]

To optimize the performance of this harvester, different anodes (Al, Cu, Zn, Fe, and Mg) and air–electrodes (Co, Ni, Au, and Pt) were investigated (see Figures S2 and S3, Supporting Information, for detailed information). Thanks to its highest power output and biocompatibility,[5] we have decided to use Mg (acceptable daily intakes of 350 mg)[33] as the anode and Pt as the cathode material.[34] **Figure 3**a–c provides the voltage, current, and load-line analysis of the Mg–O_2 harvester using a

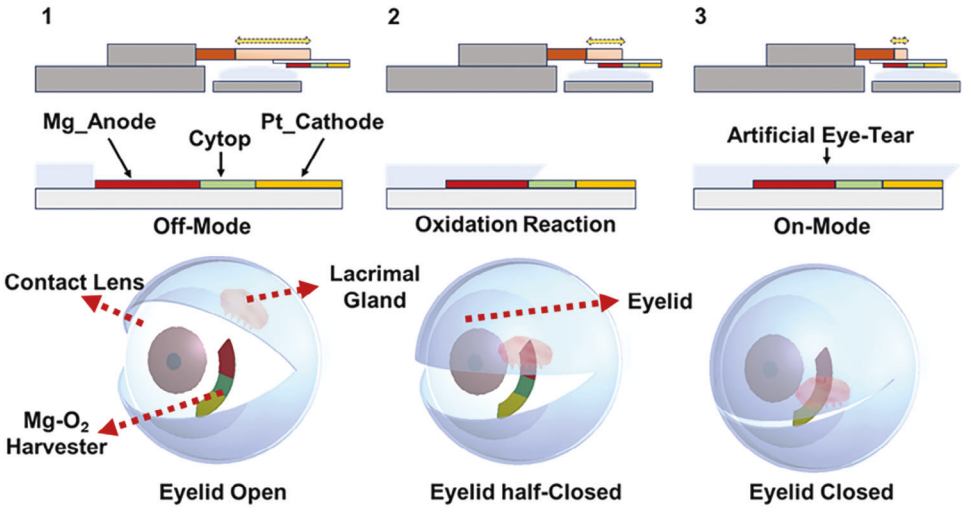

Figure 2. Linear and angular frequent motion to present the working principle of the Mg–O_2 harvester.

moisturizing eye drop as the electrolyte under linear non-stop frequent motion. The highly novel Mg–O_2 harvester delivers V_{oc}, I_{sc}, and maximum power output of 2.2 V, 1.48 mA, and 311 µW at the load of 740 Ω, corresponding to the internal impedance of the harvester.

The dynamic de-fouling mode of operation (frequent back-and-forth motion of the electrolyte on the device) results in a significantly longer battery lifetime compared to a static Mg–air battery. Dynamic de-fouling of the Mg surface occurs during the natural eye-blinking motion. When operated under dynamic de-fouling the device showed 8 times longer lifetime with a cumulative energy output of ≈8 J cm^{-2}. Considering an adult's average blinking frequency of 200 mHz (12 times per minute),[35] under natural blinking motion. There are three main reasons explaining the superior performance under dynamic mode of operation. First, the eye tear electrolyte in contact with the Mg electrode is replenished during every blinking cycle. The availability of a fresh eye tear with its natural turnover rate of 1–3 µL min^{-1} [36] guarantees a continuous supply of molecular dissolved oxygen, a constant pH, and a stable resistivity, which are key factors in energy production efficiency. Second, the open-cell configuration of our harvester provides access to a nearly unlimited source of atmospheric oxygen. Finally, the frequent motion during natural eye blinking contributes to reducing the formation rate of the passivation layer on the anode material (see Figure S4, Supporting Information, for more details).

Because of these promising results, we have implemented the eye-blinking activated Mg–O_2 harvester on a dome-shaped

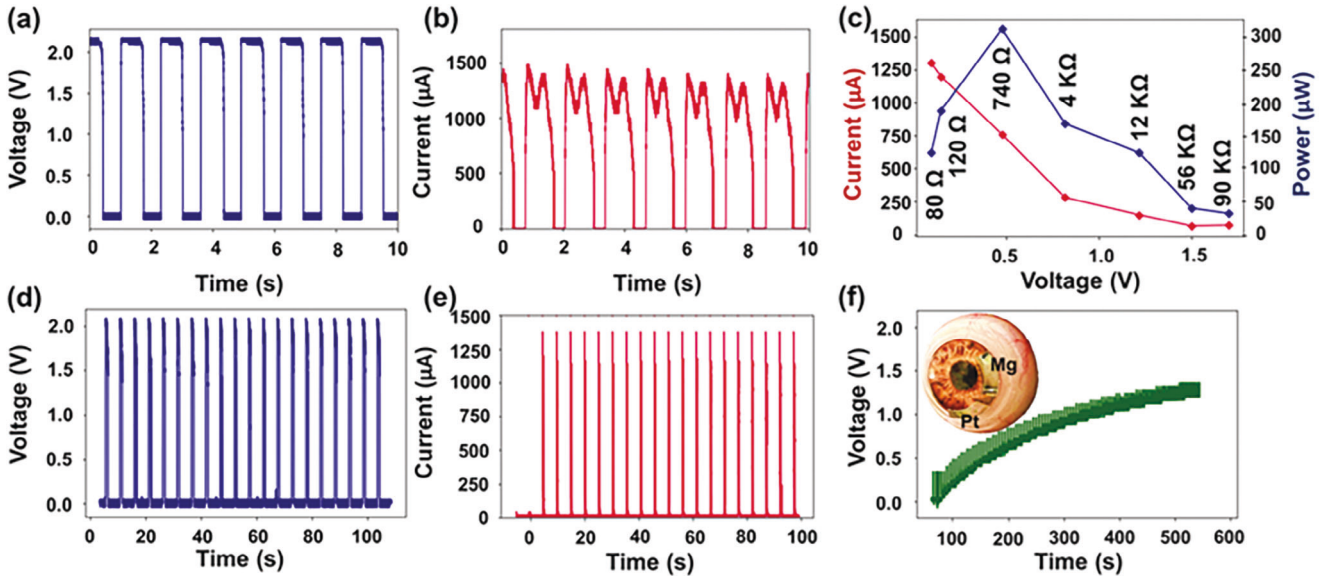

Figure 3. Electrical outputs of the eye-blinking activated Mg–O_2 harvester; a-c) linear non-stop back and forth motion, d,e) angular motion with the frequency of 200 mHz to replicate natural eye-blinking motion, f) charging curve of the 11 mF supercapacitor, inset shows the Mg–O_2 harvester mounted on a visibly-transparent PDMS contact lens.

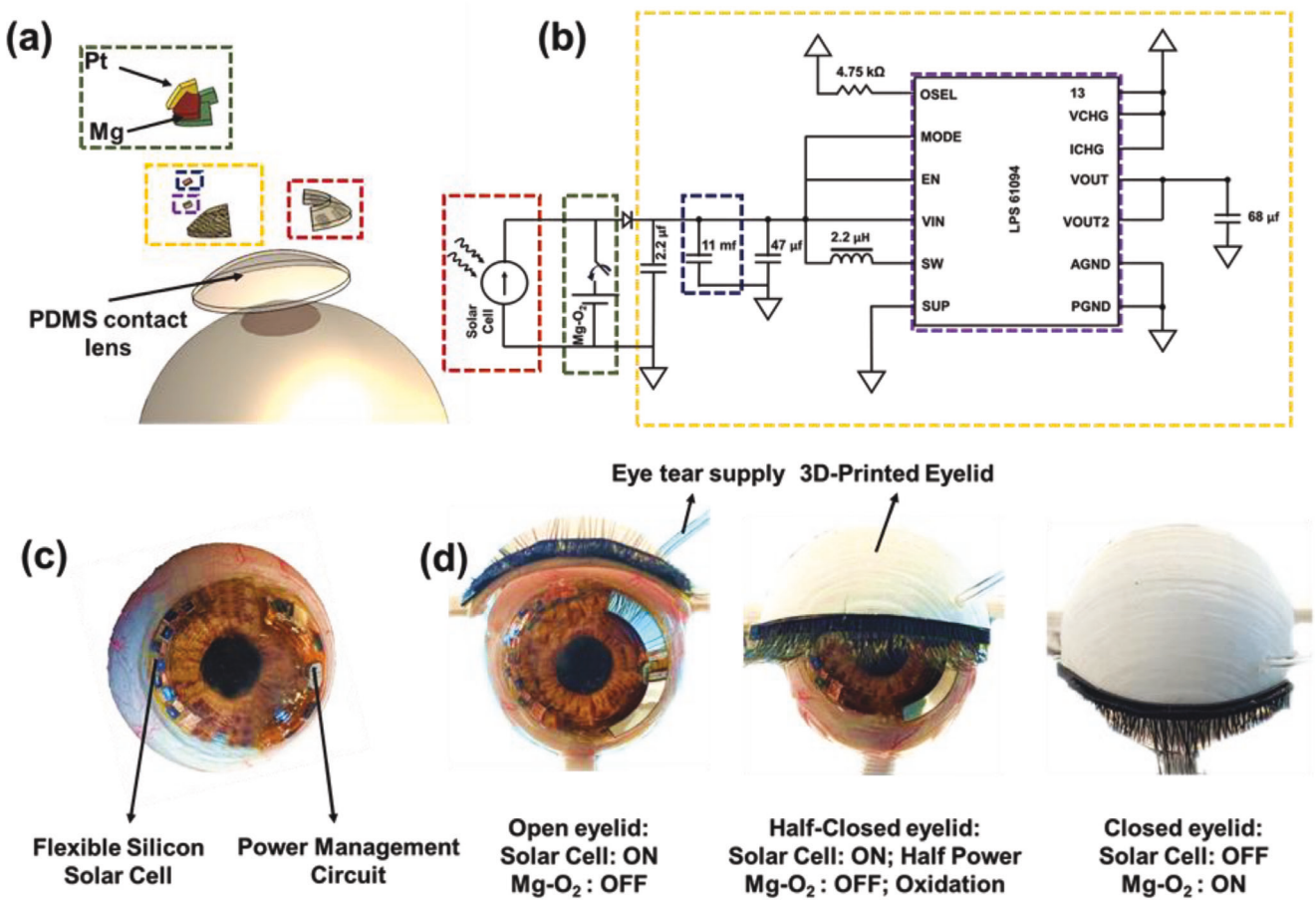

Figure 4. Integrated power pack; a) Exploded view of the flexible power pack's components, b) circuit diagram of the entire power pack, c) PDMS-encapsulated power management circuit and the flexible solar cell mounted on an eyeball replica, and d) power pack's electrical status under natural eye blinking conditions.

contact lens substrate and replicated the eye-blinking motion. As shown in Figure 3d,e, this harvester delivers V_{oc} and I_{sc} of 2.2 V and 1.4 mA, respectively. Measuring the area under the curve for the current versus time plot shows an electric charge generation of 0.3 mC per blinking cycle. As shown in Figure 3f, this harvester can charge the 11 mF supercapacitor with the internal impedance of 160 Ω, where is this coming from, very unclear (this is chosen as the energy storage unit for our power pack) from zero to 1.3 V in 8 min, corresponding to 96 blinking cycles and the delivered power of 40 µW under natural eye blinking conditions. Figure 3f also shows the flexible Mg-O_2 harvester conformally mounted on a visibly transparent PDMS contact lens substrate (for more information regarding the flexibility of the Mg-O2 harvester see Figure S5, Supporting Information).

2.3. Integrated Harvesters and Power Pack

After successful fabrication and characterization of the flexible silicon solar cell and the Mg–O_2 harvester, we integrated both energy generators with a power management circuit for three main reasons. First off, the eye-blinking activated Mg-O_2 harvester delivers a pulsed output, and due to the nature of light interruption during frequent blinking motion, the DC output of the solar cells also produces pulsed output. Our power management microsystem converts the AC outputs of the energy generators to a stable DC voltage. Second, it is of significant importance to integrate an energy storage unit to compensate for weak solar cell performance under low-intensity lighting conditions. When the energy drain is high, this microsystem uses all the generated and stored energy available to keep the load functional and while the output device or the electrical load is in the off mode, the generated energy recharges the energy storage unit. Last, our microsystem delivers 3.3 V DC output, which is a common microcontrollers' working voltage.

Figure 4a,b shows the exploded view and the circuit diagram of the power pack's stacking configuration mounted on the smart contact lens, in which the lower layer contains the solar cell and the power management unit (Figure 4c), and the Mg–O_2 harvester is placed on top of the PDMS encapsulated flexible circuit.

Figure 4d shows the power generation condition of our power pack during the natural eye blinking cycle. As shown, when the eyelids are open, the solar cell generates electrical power, while the Mg–O_2 harvester is in its off mode. When the eyelids are half-closed, since eyelids block half of the cells, the solar cell generates electricity at its half power. Finally, when the eyelids are

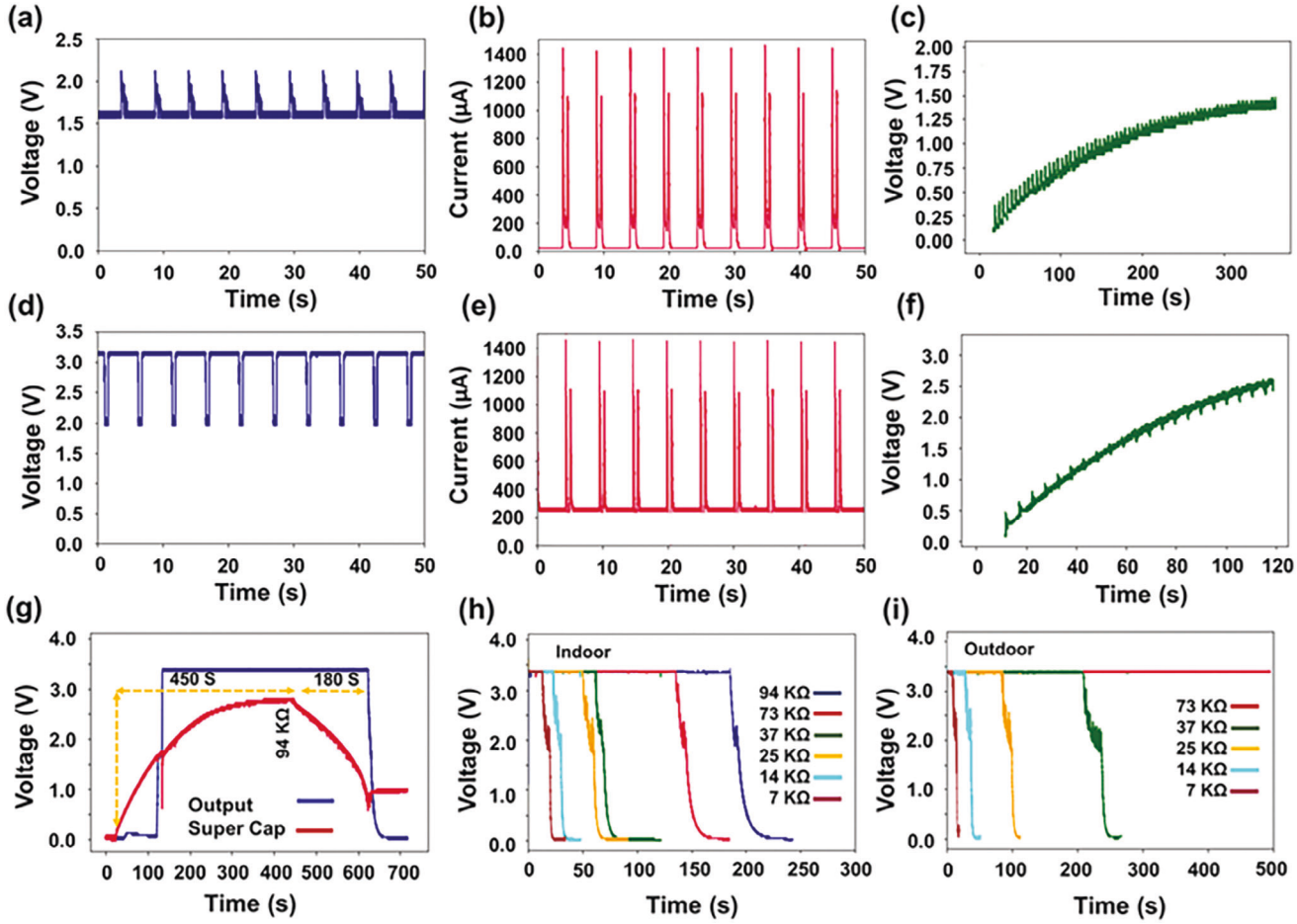

Figure 5. Integrated power pack; a–c) voltage, current, and charging curve of the 11 mF supercapacitor under indoor lighting condition, d–f) voltage, current, and charging curve of the 11 mF supercapacitor under outdoor lighting condition, g) charging of the supercapacitor using the recharging box, boosting performance of the power management IC, and power supply capability of the power pack without the energy generator unit, h,i) performance of the power pack under indoor and outdoor lighting conditions, respectively.

completely closed the solar cell stops working, but the eye tear-activated Mg–O_2 harvester generates electrical energy. Overall, unlike the wireless power transfer technique, which is the most common method to supply electricity to smart contact lenses, our power pack continuously generates electric power without the need for any external accessories.

In order to realize the integration of the two power sources with maximum efficiency, we first analyzed the effects of the generator outputs when connected to each other. Since in series connection the source rating for lower current acts upon the circuit, and the solar cell generates a minimal amount of current under indoor or low-intensity lighting, we have decided to make parallel connections between the solar cell and the eye-blinking activated Mg–O_2 harvester. Otherwise, the Mg–O_2 harvester becomes redundant. **Figure** 5a–f presents the electrical outputs of the energy generation unit. Under indoor lighting conditions, the V_{oc} is 2 V with the DC offset of 1.6 V, which is the V_{oc} of the solar cell. The I_{sc} is 1.4 mA, which is mainly supplied by the Mg–O_2 harvester. As provided in Figure 5d,e the V_{oc} changes between 2 and 3.2 V under outdoor lighting conditions, which is attributed to the voltages of the Mg–O_2 harvester and the solar cell, respectively. The maximum I_{sc} is 1.4 mA and when the Mg–O_2 harvester is in its off-mode (eyelids open), the solar cell delivers 230 μA of current. Furthermore, Figure 5c,f shows the charging curve of the 11 mF supercapacitor using this energy generator unit both under indoor and outdoor lighting conditions. It takes 360 and 110 s to charge the 11 mF supercapacitor from zero to 1.3 and 2.5 V under indoor and outdoor lighting conditions, respectively. Accordingly, the average power of this energy generator unit (comprised of the solar cell and the eye tear Mg–O_2 harvester) delivered to the 11 mF supercapacitor are 51 and 625 μW. Unlike just using the eye-tear activated Mg–O_2 harvester in which the backflow of current occurs when the generator goes to its off-mode, the parallel connection to the solar cell prevents the termination of energy generation when the eyelids are open and reduces the backflow of current from the 11 mF supercapacitor, which in turn boosts the power delivered to the energy storage unit.

Figure 5g presents the voltage boosting of the power management unit when using the recharging box. The recharging box shines a white LED light on the power pack, thus charging the 11 mF supercapacitor to 2.8 V in 450 s. During the charging cycle, as soon as the supercapacitor's voltage reaches 1.8 V (IC's

cold start), the boosting occurs and the output voltage reaches 3.3 V DC with almost no voltage ripples (As opposed to the Dickson's configuration reported in[21]).

After charging the supercapacitor and disconnecting the energy generator unit (switching off the LED), a 94 KΩ resistive load is added to the output of the power pack, showing that our microsystem can deliver 3.3 V DC voltage with a power of 115.85 µW for 180 s, which translates to a supplied electrical energy of 20.8 mJ. It should be noted that this system stops supplying 3.3 V to the output load as soon as the input (supercapacitor's voltage) drops to 0.7 V, which is the minimum required input voltage to keep the TPS 61094 operational.

It is extremely important to place a low forward voltage Schottky diode between the generator unit and the supercapacitor to prevent current backflow from the storage unit to the eye blinking activated Mg–O_2 harvester, which severely affects the power output (see Figure S6, Supporting Information, for more information). Figure 5h,i shows the power pack performance while the solar cell and the eye blinking activated Mg–O_2 harvester are connected to the input of the microsystem. As shown in Figure 5h, using the same loading (94 KΩ) under indoor lighting conditions, the power pack delivers 115.85 µW for 195 s, corresponding to the energy output of 22.6 mJ, which is approximately 8.6% higher than that of having no generators at the input. Figure 5i shows the power pack performance under outdoor lighting for different load conditions. The power pack can deliver 3.3 V DC voltage and 149.18 µW to a 73 KΩ load, continuously (Figure 4h the red line), but it can also provide higher power bursts over a short time, as may be needed for short wireless communications between the ocular microsystem and a controlling phone for example. The power pack can deliver a load power of 1.55 mW for 10 s before the energy stored in the supercapacitor is depleted. See Table S1 (Supporting Information_ for the detailed information regarding the power outputs and their delivery time.

Although for higher power outputs after a certain amount of time, the power pack pauses supplying energy to the output, it is significantly important to note that smart contact's sensors do not usually work constantly, but sometimes switch to their off-mode. For instance, our liquid crystal Fresnel lens has a duty cycle of 10–20% with the response time of just 248 milliseconds[26] and the magnetometer distance ranging system has the on/off time ratio of 0.003.[27] Accordingly, our microsystem's on-time may enhance depending on the duty cycle of a potential sensor. Basically, the generators' energy is just consumed to charge up the storage unit as soon as the load goes into its off mode. In addition, as shown in Figure S7 (Supporting Information), if the load remains on its on mode, the supercapacitor's buck up charging initiates immediately after the IC stops operating (supercapacitor's voltage 0.7 V), which helps the power pack to restart supplying energy to the load.

3. Conclusion

In this work, we have introduced an on-the-eye power scavenging energy source which delivers a sustained electrical power of 149.18 µW and a burst energy of 64.75 mJ at 3.3 V DC output without any external accessories or power sources. The energy source consists of a flexible silicon solar cell, an eye blinking activated Mg–air harvester with the lifetime of 34 d, an 11 mF supercapacitor as an energy storage unit, and a power management circuit to stabilize the output voltage for a wide range of loads. Based on our measurements, this power pack is able to continuously supply a smart contact lens for vision correction consisting of a distance ranging sensor, an I2C readout sensor, and a tunable liquid crystal lens. Our newly designed recharging box is also introduced for the first time, which can recharge the 11 mF supercapacitor to 2.8 V in just 450 s. This self-standing power pack can be utilized as a sustainable power source for optoelectronic components on smart contact lenses and pave the way for the commercialization of smart ocular devices.

4. Experimental Section

Fabrication of a Flexible Silicon Solar Cell: As illustrated in Figure S8 (Supporting Information), the fabrication process begins with boron doping (at 1000 °C for 1h) on a p-type silicon wafer to make a p++ region. Next, the silicon wafer was oxidized, and a low-pressure chemical vapor deposition (LPCVD) furnace was used to deposit 400 nm of silicon nitride (Si_XN_Y) to serve as a passivation layer against the subsequent wet etching. To thin down the silicon wafer to 100 µm, the protected wafer was placed in a KOH bath at 80 °C for backside etching (Figure S8d, Supporting Information). After 4 h, the wafer was fished out of the KOH bath and rinsed with DI water to remove any etchant and by-product residue. Phosphorous diffusion was carried out at 1000 °C for 60 min on the etched side of the wafer to make the pn junction (see the recent article for more information regarding the selection of the diffusion conditions[18]). A 400 nm aluminum (Al) was sputtered (Denton Discovery 635, plasma power = 100 W) on the phosphorous-doped region serving as the back contact. Then, the passivation layer was completely removed using CF_4/O_2 and HF, respectively. A 70 nm Si_3N_4 was sputtered on the device as an anti-reflection coating (ARC). Next, the wafer was photolithographically patterned to deposit titanium and gold (Ti/Au) on the n-side of the silicon wafer serving as top contact (Figure S8g, Supporting Information). The Disco DAD 641 dicing machine was utilized to cleave up 1.5×1.5 mm^2 devices. To boost up the V_{oc} and make the device flexible, each individual cell was attached to a 25 µm polyethylene terephthalate (PET) substrate with a piece of copper tape in between, and wire bonding was used to make a series connection between eight cells with an arc-shaped configuration. Finally, an acrylic mold was placed on the wire-bonded device and filled with polydimethylsiloxane (PDMS—made by manually mixing the 10:4 ratio of Sylgard 184 from Dow Corning and the curing agent) before encapsulating it on a dome-shaped contact lens. It should be noted that PDMS was used for the contact lens substrate and encapsulation particularly because it is biocompatible, soft, highly oxygen-permeable, and can maintain the wearer's normal vision.[37,38]

Fabrication of the Eye Blinking Activated Mg–O_2 Harvester: Magnesium (Mg) foil (purity of 99.95% with a thickness of 200 µm), platinum (Pt) (200 nm is sputtered using Denton Discovery 18), and cytop (CTL-800 M, AGC chemicals) are used as an anode, cathode, and a hydrophobic interconnect to fabricate the Mg–O_2 harvester. Detailed fabrication flow and in-depth reasoning as to why it is decided to use these specific materials are available in Figures S2,S3, and S9 (Supporting Information) and the recently published research article.[21] A commercially available moisturizing eye drop (Refresh Plus Lubricant Eye Drops containing 0.5% carboxymethylcellulose sodium as an eye lubricant) was selected to replicate the application of eye tear as the electrolyte of this metal-air harvester. According to the American Academy of Optometry, the pH of this moisturizing eye drop is the same as natural tears' pH.[39] The Firgelli_FA-RA-22-12-2 linear actuator and a servo-controlled (HiTEC; HS-82MG) 3D printed eye blinking setup are employed for proof of concept and emulation of angular eye blinking motion, respectively (Figure 2). It should be noted that in order to replicate the natural blinking conditions, the motion speed and frequency of the actuators are programmed as 15 cm s^{-1} and 200 mHz,[35] respectively.

Power Pack Integration: After fabrication and characterization of the flexible silicon solar cells and eye blinking activated Mg–O_2 harvester, a parallel connection was formed between them. The output of the energy generator unit was connected to the power management microsystem. The heart of the power management circuit is the 60 nA quiescent current bi-directional converter, TPS 61094 (13 pins— 2×3 mm^2). Although the manufacturer of the IC has its own evaluation board, to design, fabricate, and test are needed the own board particularly because the form factor of the company's evaluation board and the size of all other electrical components are too large to be placed on a smart contact lens with a very limited available area (Figure S10, Supporting Information). Figure 5 illustrates the circuit diagram of the optimized power management microsystem. Besides the IC, the second important part of this circuit is the inductor. A 2.2 µH inductor is recommended by the IC manufacturer. There is a trade-off between inductors' footprint, their saturation current, and their power efficiency within a circuit. Four different inductors, including XFL 2006, LPS 3008, LPS 4010, and LPS 4020, are populated and tested. As shown in Figure S11 (Supporting Information), under certain testing conditions, the LPS 4020 delivers the maximum energy due to its highest saturation current (20% drop) of 2.7 A. However, its thickness is 2 mm which is much beyond the acceptable thickness for the application of smart contact lenses. XFL 2006 has the lowest thickness (0.6 mm) amongst the above-mentioned inductors. However, it shows a very low power efficiency due to its low saturation current of 0.6 A. Since LPS 3008 and LPS 4010 have the same power efficiencies, to use LPS 3008 due to its lower footprint of $3 \times 3 \times 0.8$ mm^3 is decided.

Another important part of designing the power management circuit is the selection of an energy storage unit. An 11 mF CPH3225A with the nominal capacity of 4.6 µAh (Seiko Instruments Inc.) supercapacitor is selected due to its fast and easy recharging capability together with its tiny footprint and biocompatibility as opposed to Li-ion batteries. A 68 µf capacitor is utilized as the output storage unit and a 2.2 µf capacitor is populated as the input voltage regulators. Furthermore, the output DC voltage of this power management circuit is defined by changing a select resistor. Due to the output voltage requirement, which is 3.3 V, a 4.75 KΩ resistor is used.

In order to reduce the ringing effect which is induced by a load step at the output, a 47 µf capacitor ($T = 0.8$ mm) between the ceramic input capacitor and the power source (see Figure S12, Supporting Information, for more information) is populated. A RB521VM-40TE-17 Schottky diode was used in between the energy generator and storage units to prevent any current backflow from the storage unit to the generator.

A rigid PCB was designed and fabricated to populate all the components stated above. After successful characterization of the circuit on the rigid board, a flexible PCB was designed and fabricated to be able to encapsulate the power management microsystem within a curved PDMS contact lens without any mechanical and electrical degradation.

Characterization Techniques: A NanoSpec 3000 small spot spectroscopic reflectometer was used to measure the thickness of SiO_2 and Si_xN_y throughout the fabrication process. The sheet resistance of the p and n-type silicon was measured using the Microtech RF-1 4-point probe. Photocurrent density–voltage (*J–V*) measurements were conducted both under standard one sun (AM1.5) and indoor light conditions. The Oriel Sol3A and a white light LED were used for simulating the sun's light and indoor light, respectively. In addition, the Hewlett-Packard precision parameter analyzer 4145A was used to collect the *IV* results and the internal impedance of the Mg–O_2 harvester. It should also be noted that the light power of the indoor source was measured and calibrated using a digital optical power meter from THORLABS Co (Model PM100D).

A Tencor P-10 profilometer was used to measure the thickness of the electrodes and the Cytop. All voltages were measured by probing the electrodes of the devices using a digital oscilloscope (Siglent SDS1202X-E) with an input impedance of 1 MΩ and an input capacitance of 15 pF. The short circuit current output of the devices was measured using a Stanford Research Systems (SR570) low noise preamplifier with a DC input impedance of 1Ω for a sensitivity of 500 µA V^{-1}.

Supporting Information

Supporting Information is available from the Wiley Online Library or from the author.

Acknowledgements

All the fabrication was performed at the state-of-art Utah Nano Fabrication Facility, Salt Lake City, Utah, USA sponsored under NSF CPS grant 10053422.

Conflict of Interest

The authors declare no conflict of interest.

Data Availability Statement

The data that support the findings of this study are available in the supplementary material of this article.

Keywords

eye-blinking, metal–air batteries, power pack, smart contact lenses, solar cells

Received: February 11, 2024
Revised: March 2, 2024
Published online:

[1] M. Elsherif, R. Moreddu, F. Alam, A. E. Salih, I. Ahmed, H. Butt, *Front. Med.* **2022**, *9*, 858784.
[2] D. H. Keum, S.-K. Kim, J. Koo, G.-H. Lee, C. Jeon, J. W. Mok, B. H. Mun, K. J. Lee, E. Kamrani, C.-K. Joo, S. Shin, J.-Y. Sim, D. Myung, S. H. Yun, Z. Bao, S. K. Hahn, *Sci. Adv.* **2020**, *6*, eaba3252.
[3] J. Zhang, K. Kim, H. J. Kim, D. Meyer, W. Park, S. A. Lee, Y. Dai, B. Kim, H. Moon, J. V. Shah, K. E. Harris, B. Collar, K. Liu, P. Irazoqui, H. Lee, S. A. Park, P. S. Kollbaum, B. W. Boudouris, C. H. Lee, *Nat. Commun.* **2022**, *13*, 5518.
[4] H. Torun, B. Fazla, S. Arman, B. Ozdalgic, A. K. Yetisen, S. Tasoglu, *Nano Sel.* **2023**, *4*, 79.
[5] S. Kusama, K. Sato, S. Yoshida, M. Nishizawa, *Adv. Mater. Technol.* **2020**, *5*, 1900889.
[6] J. Jang, J. Kim, H. Shin, Y.-G. Park, B. J. Joo, H. Seo, J. Won, D. W. Kim, C. Y. Lee, H. K. Kim, J.-U. Park, *Sci. Adv.* **2021**, *7*, eabf7194.
[7] A. Banerjee, C. Ghosh, M. Karkhanis, A. Deshpande, E. Pourshaban, H. Kim, C. H. Mastrangelo, in *Conf. Lasers Electro-Optics, 2022 Paper AW4C3*, Optica Publishing Group, IEEE Xplore, Washington, DC **2022**, pp. 1–2.
[8] C. Ghosh, A. Banerjee, M. Karkhanis, E. Pourshaban, H. Kim, C. H. Mastrangelo, A. Deshpande, in *2022 IEEE Photonics Conf. IPC*, IEEE Xplore, Piscataway, NJ **2022**, pp. 1–2.
[9] M. X. Chu, K. Miyajima, D. Takahashi, T. Arakawa, K. Sano, S. Sawada, H. Kudo, Y. Iwasaki, K. Akiyoshi, M. Mochizuki, K. Mitsubayashi, *Talanta* **2011**, *83*, 960.
[10] J. Park, J. Kim, S.-Y. Kim, W. H. Cheong, J. Jang, Y.-G. Park, K. Na, Y.-T. Kim, J. H. Heo, C. Y. Lee, J. H. Lee, F. Bien, J.-U. Park, *Sci. Adv.* **2018**, *4*, eaap9841.
[11] T. Takamatsu, Y. Chen, T. Yoshimasu, M. Nishizawa, T. Miyake, *Adv. Mater. Technol.* **2019**, *4*, 1800671.

[12] C. Yang, Q. Wu, J. Liu, J. Mo, X. Li, C. Yang, Z. Liu, J. Yang, L. Jiang, W. Chen, H. Chen, J. Wang, X. Xie, *Nat. Commun.* **2022**, *13*, 2556.
[13] J. Kim, M. Kim, M.-S. Lee, K. Kim, S. Ji, Y.-T. Kim, J. Park, K. Na, K.-H. Bae, H. Kyun Kim, F. Bien, C. Young Lee, J.-U. Park, *Nat. Commun.* **2017**, *8*, 14997.
[14] H. Mirzajani, F. Mirlou, E. Istif, R. Singh, L. Beker, *Biosens. Bioelectron.* **2022**, *197*, 113761.
[15] T. Takamatsu, Y. Sijie, F. Shujie, L. Xiaohan, T. Miyake, *Adv. Funct. Mater.* **2020**, *30*, 1906225.
[16] M. H. M. Kouhani, J. Wu, A. Tavakoli, A. J. Weber, W. Li, *Lab Chip* **2020**, *20*, 332.
[17] E. Pourshaban, M. U. Karkahnis, A. Deshpande, M.d. R. Hasan, N. D. Rock, A. Banerjee, C. Ghosh, H. Kim, C. H. Mastrangelo, in *2022 21st Int. Conf. on Micro and Nanotechnology for Power Generation and Energy Conversion Applications (PowerMEMS)*, IEEE Xplore, Piscataway, NJ **2022**, pp. 264–266.
[18] E. Pourshaban, A. Banerjee, A. Deshpande, C. Ghosh, M. U. Karkhanis, R. Hasan, N. D. Rock, H. Kim, C. H. Mastrangelo, *ACS Appl. Electron. Mater.* **2022**, *4*, 4016.
[19] E. Pourshaban, A. Banerjee, C. Ghosh, A. Deshpande, H. kim, C. Mastrangelo, in *2021 IEEE 48th Int. Conf. on Photovoltaic PVSC*, IEEE Xplore, Piscataway, NJ **2021**, pp. 1897–1900.
[20] E. Pourshaban, A. Banerjee, C. Ghosh, A. Deshpande, H. Kim, C. H. Mastrangelo, in *2021 IEEE 34th Int. Conf. on Micro Electro Mechanical Systems MEMS*, IEEE Xplore, Piscataway, NJ **2021**, pp. 246–249.
[21] E. Pourshaban, A. Banerjee, M. U. Karkhanis, A. Deshpande, C. Ghosh, H. Kim, C. H. Mastrangelo, *Adv. Mater. Technol.* **2023**, *8*, 2200518.
[22] E. Pourshaban, A. Deshpande, M. U. Karkhanis, A. Banerjee, C. Ghosh, H. Kim, C. H. Mastrangelo, in *2022 IEEE 35th Int. Conf. on Micro Electro Mechanical Systems MEMS*, IEEE Xplore, Piscataway, NJ **2022**, pp. 608–611.
[23] E. Pourshaban, M. U. Karkhanis, A. Deshpande, A. Banerjee, H. Kim, C. H. Mastrangelo, in *2021 IEEE Sensors*, IEEE Xplore, Piscataway, NJ **2021**, pp. 1–4.
[24] E. Pourshaban, M. Karkhanis, A. Deshpande, A. Banerjee, C. Ghosh, H. Kim, C. Mastrangelo, in *2021 IEEE Int. Conf. on Flexible, Printable Sensors and Systems*, IEEE Xplore, Piscataway, NJ **2021**, pp. 1–4.
[25] E. Pourshaban, M. Karkhanis, A. Deshpande, A. Banerjee, C. Ghosh, H. Kim, C. Mastrangelo, in *2021 IEEE 21st Int. Conf. on Solid-State Sensors, Actuators, and Microsystems Transducers*, IEEE Xplore, Piscataway, NJ **2021**, pp. 960–963.
[26] A. Banerjee, C. Ghosh, M. U. Karkhanis, A. Deshpande, E. Pourshaban, A. Majumder, H. Kim, C. H. Mastrangelo, *Opt. Express* **2023**, *31*, 17027.
[27] A. Deshpande, M. U. Karkhanis, C. Ghosh, E. Pourshaban, M.d. R. Hasan, A. Banerjee, H. Kim, C. H. Mastrangelo, *IEEE Access* **2023**, *11*, 28596.
[28] S.-W. Hwang, G. Park, C. Edwards, E. A. Corbin, S.-K. Kang, H. Cheng, J.-K. Song, J.-H. Kim, S. Yu, J. Ng, J. E. Lee, J. Kim, C. Yee, B. Bhaduri, Y. Su, F. G. Omennetto, Y. Huang, R. Bashir, L. Goddard, G. Popescu, K.-M. Lee, J. A. Rogers, *ACS Nano* **2014**, *8*, 5843.
[29] C. Battaglia, A. Cuevas, S. D. Wolf, *Energy Environ. Sci.* **2016**, *9*, 1552.
[30] S. Wu, Z. Li, M.-Q. Li, Y. Diao, F. Lin, T. Liu, J. Zhang, P. Tieu, W. Gao, F. Qi, X. Pan, Z. Xu, Z. Zhu, A. K.-Y. Jen, *Nat. Nanotechnol.* **2020**, *15*, 934.
[31] P. Kiyat, M. Palamar, B. Gerceker Turk, A. Yagci, *Cornea* **2020**, *39*, 1108.
[32] N. Knop, E. Knop, *Ophthalmologe* **2009**, *106*, 872.
[33] C. J. Bettinger, *Trends Biotechnol.* **2015**, *33*, 575.
[34] F. Ekici, Ş. Korkmaz, E. E. Karaca, S. Sül, H. A. Tufan, B. Aydın, E. Dileköz, *Int. Scholarly Res. Not.* **2014**, *2014*, 745439.
[35] K.-A. Kwon, R. J. Shipley, M. Edirisinghe, D. G. Ezra, G. Rose, S. M. Best, R. E. Cameron, *J. R. Soc. Interface* **2013**, *10*, 20130227.
[36] D. Dartt, M. Willcox, *Exp. Eye Res.* **2013**, *117*, 1.
[37] J. Chuan Yeo, Kenry, C. Teck Lim, *Lab Chip* **2016**, *16*, 4082.
[38] X. Ma, S. Ahadian, S. Liu, J. Zhang, S. Liu, T. Cao, W. Lin, D. Wu, N. R. de Barros, M. R. Zare, S. E. Diltemiz, V. Jucaud, Y. Zhu, S. Zhang, E. Banton, Y. Gu, K. Nan, S. Xu, M. R. Dokmeci, A. Khademhosseini, *Adv. Intell. Syst.* **2021**, *3*, 2000263.
[39] L. G. Carney, T. F. Mauger, R. M. Hill, *Invest. Ophthalmol. Visual Sci.* **1989**, *30*, 747.